Synthesis and characterization of 'double-cubane' complexes containing MFe_3Se_4 cores (M = Mo, W)

Mark A. Greaney*, Catherine L. Coyle, Robert S. Pilato and Edward I. Stiefel
Exxon Research and Engineering Company, Route 22 East, Annandale, NJ 08801 (USA)

(Received June 18, 1991)

Abstract

The reaction system $(Et_4N)_2MSe_4$ (M = Mo, W)/$FeCl_3$/EtSH/Na in methanol or ethanol at ambient temperature has yielded three principal products: $[M_2Fe_6Se_8(SEt)_9]^{3-}$, $[M_2Fe_7Se_8(SEt)_{12}]^{3-}$ (M = Mo, W); and $[W_2Fe_7Se_8(SEt)_{12}]^{4-}$ which are isolable as Et_4N^+ salts. The structure of $(Et_4N)_3[Mo_2Fe_6Se_8(SEt)_9]$ has been determined by single-crystal X-ray diffraction. It crystallizes in the hexagonal space group $P6_3/m$ with $a = 17.453(3)$, $c = 16.575(2)$ Å and $Z = 2$. Reaction of $[Mo_2Fe_7Se_8(SEt)_{12}]^{3-}$ with 6 equiv of acetyl chloride or arylthiol afforded new clusters with substitution of the terminal ethanethiolate ligands: $[Mo_2Fe_7Se_8(SEt)_6Cl_6]^{3-}$ and $[Mo_2Fe_7Se_8(SEt)_6(SC_6H_4X)_6]^{3-}$, X = H, Cl. The structure of $(Et_4N)_3[Mo_2Fe_7Se_8(SEt)_6(SC_6H_4Cl)_6$ has been determined by single crystal X-ray diffraction. It crystallizes in the space group $P\bar{1}$ (No. 2) with $a = 11.401(2)$, $b = 12.697(2)$, $c = 19.897(3)$ Å, $\alpha = 87.91(1)$, $\beta = 74.93(1)$, $\gamma = 89.14(2)°$ and $Z = 1$. The anions in both structures are of the 'double-cubane' type containing trigonally distorted $MoFe_3Se_4$ subclusters which are linked through the Mo atoms. In the former, linkage is through three μ_2-ethanethiolate ligands; whereas in the latter, the bridging is accomplished by a $Fe(SEt)_6$ distorted trigonal anti-prismatic moiety. These complexes are structurally similar to the related sulfur double-cubanes. Incorporation of the larger selenide ion has a surprisingly small effect upon the M···Fe distances within the cubane subclusters. All products show the full stoichiometric amount of four selenium atoms per cubane unit, indicating that MSe_4^{2-} can effectively deliver all four selenium atoms in the assembly process even though one is no longer covalently bound to M. All clusters exhibit isotropically shifted ^1H NMR spectra, which are the result of both contact and dipolar shift mechanisms and are larger in magnitude than the shifts observed in the sulfur analogs. This is consistent with the larger solution magnetic moments of these selenium double-cubanes as determined by the Evans method. Electrochemical reduction potentials of these selenium double-cubanes were nearly identical to their sulfur analogs as determined by cyclic voltammetry. Full tabulation of ^1H NMR isotropic shifts, electronic absorption maxima, electrochemical reduction potentials, room temperature solution magnetic susceptibilities, and representative cyclic voltammograms and ^1H NMR spectra are presented.

Introduction

In the last decade, research directed at producing models of the catalytic site of the enzyme nitrogenase has resulted in the synthesis of structurally diverse iron, molybdenum and sulfur-containing clusters [1]. Nearly simultaneously, Holm and co-workers [2] and Christou *et al.* [3] reported 'self-assembly' reactions that led to the first of the double-cubane clusters **1** and **2**. Subsequently, double-cubane types **3** and **4** were reported [4] which in turn provided access to the 'mono-cubane' clusters, which are good spectroscopic models for the active site in nitrogenase [5]. More recently, the type **3** double-cubane structure has been synthesized with substitution of Mo by V [6] or Re [7] demonstrating the general nature of this structural type. The common 'self-assembly' synthetic pathway to the double-cubane clusters involves the reaction of MS_4^{2-}, $FeCl_3$ and RS^- in alcoholic solutions, although the mechanistic details have not been delineated.

Early work by Müller *et al.* has shown the similarity in reactivity of WSe_4^{2-} relative to its sulfur analog in the complex, $(PPh_3)_3Ag_2(WSe_4)$, in which WSe_4^{2-} acts as a bidentate ligand, retains its tetrahedral structure and undergoes no change in oxidation state [8]. Recently, convenient methods for the production of the tetraselenometallate dianion, MSe_4^{2-} (M = Mo, W), have renewed interest in the chemistry of these species [9]. For example, Rauchfuss and

*Author to whom correspondence should be addressed.

0020-1693/91/$3.50

© 1991 — Elsevier Sequoia, Lausanne

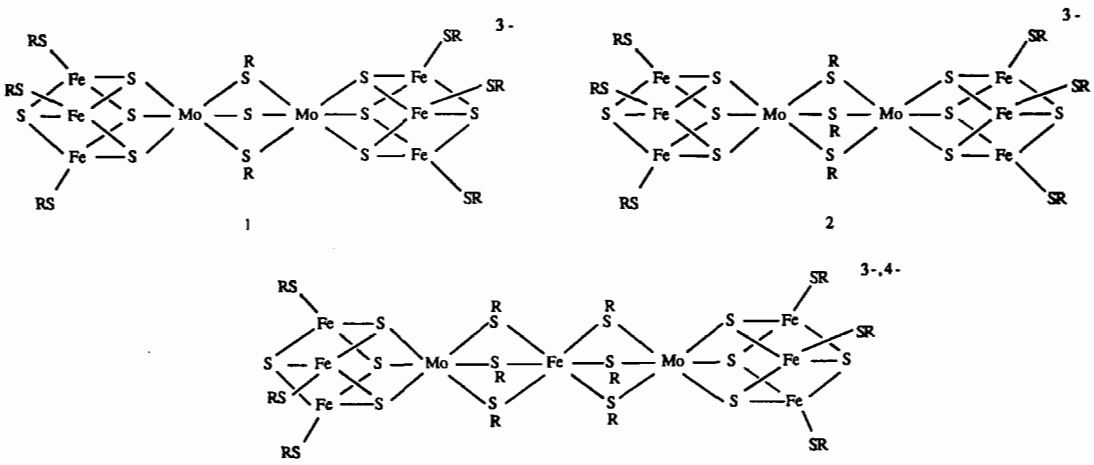

3 (3-) , 4 (4-)

co-workers, have reported the synthesis of $(MeCp)_2Ru_2(PPh_3)_2(MSe_4)$ in which MSe_4^{2-} is coordinated to Ru in a manner identical to its sulfur analog [10]. Similarly, Müller *et al.* have reported several structures in which the tetraselenometallate dianions have coordinated similarly to the tetrasulfido analogs [11]. Clearly the behavior of MX_4^{2-} (X = S, Se) as a ligand is apparently very similar, however, the chemical reactivity is not. For example, Ibers and co-workers have reported several tungsten selenide cluster complexes for which no sulfide analog is known [12]. These complexes were synthesized from WSe_4^{2-} under similar reaction conditions to those used for WS_4^{2-} but yielded dissimilar products demonstrating a significant difference in reactivity of the tetraselenometallate dianion relative to its sulfido analog.

We undertook a research program to investigate whether the MSe_4^{2-} dianion would participate in the 'self-assembly' type reactions to produce selenium double-cubanes or some other cluster complexes. Holm and coworkers have shown that it is possible to replace some or all of the sulfide atoms with selenide atoms in the related thio-cubane $Fe_4S_4(SR)_4^{2-}$ clusters by direct reaction of elemental selenium in place of elemental sulfur [13]. In our study, the source of the selenium is the tetraselenometallate dianion. Can MSe_4^{2-} effectively deliver all four selenium atoms in the assembly process even though one selenium is no longer covalently bound to M? If selenium double-cubanes were produced they could provide information of relevance to known selenium-containing enzymes [14]. They could also provide further insights into the mechanism of the 'self-assembly' type reactions and the magnetic and electronic properties of the active site of nitrogenase. Moreover, ^{77}Se (natural abundance = 8%), which has a nuclear spin of 1/2, could provide a spectroscopic handle unavailable in the sulfur analogs.

Experimental

Measurements

All measurements were performed under anaerobic conditions with solvents purified by standard techniques and degassed prior to use. Electronic absorption spectra were recorded on a Perkin-Elmer model 330 spectrophotometer. Cyclic voltammetric studies were performed with a BAS 100 electrochemical analyzer and an IBM voltammetric cell consisting of a glassy-carbon working electrode (area = 16 mm^2), a platinum wire auxiliary electrode, and a saturated calomel reference electrode. ^1H NMR spectra were recorded on a Bruker WM-360 spectrometer equipped with a deuterium lock and a variable temperature controller calibrated to ± 1 °C with an ethylene glycol standard. Chemical shifts downfield and upfield of Me_4Si reference are designated as negative and positive, respectively. Solution magnetic susceptibilities were determined by the Evans NMR method [15] as adapted to a high-field superconducting NMR spectrometer [16], utilizing Wilmad no. 536 coaxial tubes and Me_4Si as the reference signal. Elemental analyses were performed by Galbraith Analytical Laboratory Inc., Knoxville, TN.

Single-crystal X-ray structural determinations were performed by Dr C. S. Day of Crystalytics Co., Lincoln, NE.

Materials

Potassium (99.99) and selenium (99.999) were obtained from Aesar. Sodium, ethanethiol, *p*-chloro-

thiophenol, tetraethylammonium bromide (gold label), acetyl chloride, anhydrous ferric chloride, CD_3CN and celite were obtained from Aldrich Chemical Co. and used as received. All solvents used in this study were obtained from Burdick and Jackson and were stored over molecular sieves

Syntheses

All syntheses were performed under an argon atmosphere by employing standard Schlenk-line and glove-box techniques. The basic procedures and stoichiometries were based upon the syntheses previously reported for the analogous sulfur compounds [1a, 3].

K_2Se_3

Potassium metal (0.73 g, 2.0 mmol) and elemental selenium (2.3 g, 3.0 mmol) were loaded in a glove box into a thick-walled (13 mm o.d.×20 cm×1.2 mm wall thickness) quartz glass tube which was sealed on one end. This was stoppered and brought out of the box and flame-sealed. Several such tubes can be prepared simultaneously. These tubes were then heated slowly (6 h) to 350 °C in a tube furnace equipped with a programmable temperature controller. **Caution**: this reaction is highly exothermic. Carefully sealed thick-walled quartz tubing and slow heating are critical to avoid rupture of the quartz tubes. The tubes were maintained at 350 °C for 6 h and then cooled to room temperature. The black microcrystalline product was isolated in a glove box by opening one end of the quartz tube and scraping the sides with a spatula. Typically 2.8 g (85%) of product can be scraped from the sides of the tubes.

$(Et_4N)_2[MoSe_4]$

Molybdenum hexacarbonyl (9.0 g, 34 mmol), Et_4NBr (15.0 g, 71.4 mmol) and K_2Se_3 (11.0 g, 34.9 mmol) were combined in a Schlenk flask, 200 ml dimethylformamide and 20 ml heptane were added, and the flask was fitted with a water-cooled reflux condenser. The reaction mixture was stirred vigorously and heated at 95 °C for 90 min producing a dark blue–green solution. The reaction mixture was filtered and then 300 ml of tetrahydrofuran was layered onto the filtrate and the product was allowed to crystallize further at −20 °C overnight. The crystalline turquoise product was isolated by filtration, rinsed with THF, then ether. Yield 16.1 g (69%). An analytical sample was produced by recrystallization from CH_3CN/ether. *Anal.* Calc. for $C_{16}H_{40}N_2MoSe_4$: C, 28.60; H, 5.95; N, 4.17; Se, 47.00; Mo, 14.28. Found: C, 28.42; H, 5.76; N, 3.87; Se, 46.92; Mo, 14.04%.

$(Et_4N)_2[WSe_4]$

The procedure and molar ratios in the preceding preparation were utilized in the synthesis of this compound except for the substitution of tungsten hexacarbonyl (12.0 g, 34 mmol) for molybdenum hexacarbonyl. An orange microcrystalline product was obtained. Yield 16.3 g (65%). An analytical sample was produced by recrystallization from CH_3CN/ether. *Anal.* Calc. for $C_{16}H_{40}N_2WSe_4$: C, 25.29; H, 5.26; N, 3.68; Se, 41.57; W, 24.20. Found: C, 25.23; H, 4.81; N, 3.44; Se, 42.03; W, 23.88%.

$(Et_4N)_3[Mo_2Fe_6Se_8(SEt)_9]$

A sodium ethanethiolate solution was produced by reacting 1.33 g (58 mmol) of sodium metal with 70 ml absolute methanol and then adding 4.2 ml (58 mmol) ethanethiol. Addition of this solution to a filtered solution of $FeCl_3$ (2.78 g, 17 mmol) in 70 ml methanol followed by a slurry of $(Et_4N)_2[MoSe_4]$ (3.88 g, 6.4 mmol) in 70 ml methanol produced a dark brown–green reaction mixture which was allowed to stir/react at ambient temperature overnight. After filtration, all volatile materials were removed *in vacuo*. The dark tarry residue was extracted with 60 ml of CH_3CN at 50 °C and then filtered through Celite. Volume reduction of the filtrate to 10 ml followed by cooling for 4 h at −20 °C produced a black crystalline solid which was isolated by filtration. Two recrystallizations from CH_3CN/ether produced 1.5 g (22%) of pure product. *Anal.* Calc. for $C_{42}H_{105}Fe_6Mo_2N_3S_9Se_8$: C, 24.02; H, 5.00; N, 2.00; Se, 30.12; Mo, 9.15. Found: C, 24.37; H, 5.30; N, 1.98; Se, 29.95; Mo, 9.07%. $\mu = 6.01\ \mu_B$ (CH_3CN, 295 K).

$(Et_4N)_3[W_2Fe_6Se_8(SEt)_9]$

The procedures and molar ratios in the preceding preparation were utilized in the synthesis of this compound except for the substitution of 4.86 g (6.4 mmol) of $(Et_4N)_2[WSe_4]$ for $(Et_4N)_2[MoSe_4]$. The pure product was obtained as black microcrystals after three recrystallizations from CH_3CN/ether. Yield 1.7 g (24%). *Anal.* Calc. for $C_{42}H_{105}Fe_6N_3S_9Se_8W_2$: C, 22.18; H, 4.62; N, 1.85; Se, 27.77; W, 16.17. Found: C, 22.34; H, 4.87; N, 1.91; Se, 27.23; W, 16.01%. $\mu = 5.65\ \mu_B$ (CH_3CN, 295 K).

$(Et_4N)_3[Mo_2Fe_7Se_8(SEt)_{12}]$

A sodium ethanethiolate solution was prepared by reacting sodium metal (2.46 g, 107 mmol) with 150 ml of absolute ethanol and then ethanethiol (8.2 ml, 107 mmol). This solution was then transferred into a filtered solution of $FeCl_3$ (35.06 g, 31.2 mmol) in 150 ml absolute ethanol. A slurry of $(Et_4N)_2[MoSe_4]$ (6.0 g, 8.92 mmol) in 150 ml of absolute ethanol

was then added. Crystalline material became visible within 10 min in the dark brown reaction mixture which was left to stir overnight at ambient temperature. The dark blue–black reaction product was isolated by filtration, washed with ethanol and ether and dried under vacuum. Extraction with 100 ml warm CH_3CN (75 °C), filtration through Celite and volume reduction to 30 ml afforded 4.86 g (48%) of black crystalline product. An analytical sample was produced by one further recrystallization from 2:1:1 CH_3CN: ether: THF. *Anal.* Calc. for $C_{48}H_{120}Fe_7Mo_2N_3S_{12}Se_8$: C, 24.66; H, 5.13; N, 1.80; Se, 27.02; Mo, 8.21. Found: C, 24.02; H, 5.00; N, 2.00; Se, 27.32; Mo, 7.90%. $\mu = 5.92$ μ_B (CH_3CN, 295 K).

$(Et_4N)_3[Mo_2Fe_7Se_8(SEt)_6(SC_6H_4Cl)_6]$

To a solution of $(Et_4N)_3[Mo_2Fe_7Se_8(SEt)_{12}]$ (0.50 g, 0.22 mmol) in 15 ml of CH_3CN was added *p*-chlorothiophenol (0.22 g, 1.5 mmol) in 10 ml CH_3CN. The solution immediately darkened to a deep red color. The reaction mixture was evacuated periodically to remove the displaced ethanethiol and allowed to stir for 2 h at ambient temperature. Volume reduction to 10 ml and filtration afforded a pure black microcrystalline product (0.48 g, 72%). An analytical sample was produced by recrystallization from CH_3CN/ether. *Anal.* Calc. for $C_{72}H_{114}Cl_6Fe_7Mo_2N_3S_{12}Se_8$: C, 30.53; H, 4.02; N, 1.48; Se, 22.30; Mo, 6.77. Found: C, 30.42; H, 3.89; N, 1.34; Se, 22.59; Mo, 6.84%.

$(Et_4N)_3[Mo_2Fe_7Se_8(SEt)_6Cl_6]$

A slurry of $(Et_4N)_3[Mo_2Fe_7Se_8(SEt)_{12}]$ (0.287 g, 0.125 mmol) in 20 ml CH_3CN was warmed to 50 °C to dissolve and then was treated with acetyl chloride (70 μl, 0.875 mmol) in 5 ml CH_3CN. This caused the solution to lighten noticeably, with crystals visible within 10 min. Periodic evacuation of the reaction mixture over the course of the 2 h reaction at ambient temperature was followed by volume reduction to 5 ml. The crystalline product was isolated by filtration and rinsed with 2:1 THF:CH_3CN and then ether. Yield 0.21 g (77%). *Anal.* Calc. for $C_{36}H_{70}Cl_6Fe_7Mo_2N_3S_6Se_8$: C, 19.80; H, 4.12; N, 1.92; Se, 28.92; Mo, 8.79. Found: C, 19.85; H, 4.20; N, 1.96; Se, 28.78; Mo, 8.69%.

$(Et_4N)_3[Mo_2Fe_7Se_8(SEt)_6(SC_6H_5)_6]$

The same procedure and molar ratios as used in the synthesis of $(Et_4N)_3[Mo_2Fe_7Se_8(SEt)_6(SC_6H_4Cl)_6]$ were employed in the synthesis of this complex except for the substitution of 150 μl (1.5 mmol) of benzenethiol for the *p*-chlorothiophenol. Yield 0.42 g (72%). *Anal.* Calc. for $C_{72}H_{120}Fe_7Mo_2N_3S_{12}Se_8$: C, 32.93; H, 4.57; N, 1.60; Se, 24.05; Mo, 7.31. Found: C, 32.67; H, 4.45; N, 1.54; Se, 24.31; Mo, 7.44%.

$(Et_4N)_3[W_2Fe_7Se_8(SEt)_{12}]$

The procedures and molar ratios in the preparation of $(Et_4N)_3[Mo_2Fe_7Se_8(SEt)_{12}]$ were utilized in the synthesis of this compound except for the substitution of 6.76 g (8.92 mmol) of $(Et_4N)_2[WSe_4]$ for $(Et_4N)_2[MoSe_4]$. The pure product was obtained as black microcrystals after three recrystallizations from CH_3CN/ether. Yield 4.63 g (41%). *Anal.* Calc. for $C_{48}H_{120}Fe_7N_3S_{12}Se_8W_2$: C, 22.92; H, 4.77; N, 1.66; Se, 25.13; W, 14.64. Found: C, 22.94; H, 4.87; N, 1.71; Se, 24.93; W, 14.47%. $\mu = 5.86$ μ_B (CH_3CN, 295 K).

$(Et_4N)_4[W_2Fe_7Se_8(SEt)_{12}]$

A sodium ethanethiolate solution was prepared by reacting sodium metal (0.91 g, 40 mmol) with 95 ml of absolute ethanol and then ethanethiol (2.3 ml, 40 mmol). This solution was then transferred into a filtered solution of $FeCl_3$ (2.22 g, 13.7 mmol) in 95 ml absolute ethanol. A slurry of $(Et_4N)_2[WSe_4]$ (3.0 g, 3.95 mmol) in 50 ml of absolute ethanol was then added. Crystalline material became visible within 10 min in the dark brown reaction mixture which was left to stir overnight at ambient temperature. The dark blue–black reaction product was isolated by filtration, washed with ethanol and ether and dried under vacuum. Extraction with 100 ml warm CH_3CN (75 °C), filtration through Celite and volume reduction to 30 ml afforded 2.0 g (38%) of black crystalline product. Contamination with the oxidation product $[W_2Fe_7Se_8(SEt)_{12}]^{3-}$, which is readily detected by ^1H NMR, was reduced by washing the recrystallized product with a 1 mM sodium acenapthalenide solution in HMPA (3×20 ml) followed by absolute ethanol. An analytical sample was produced by one further recrystallization from 2:1:1 CH_3CN:ether:THF. *Anal.* Calc. for $C_{56}H_{140}Fe_7N_4S_{12}Se_8W_2$: C, 25.44; H, 5.30; N, 2.12; Se, 23.89; W, 13.91. Found: C, 25.18; H, 5.12; N, 2.01; Se, 23.98; W, 13.97%. $\mu = 10.3$ μ_B (CH_3CN, 295 K).

Solution and refinement of the structure of $(Et_4N)_3[Mo_2Fe_6Se_8(SEt)_9]$

Black rectangular parallelepiped-shaped crystals were grown by slow diffusion of tetrahydrofuran into an acetonitrile solution of the complex at room temperature. A single crystal was mounted inside a glass capillary with mother liquor under a nitrogen atmosphere and oriented with its longest edge nearly parallel to the phi axis of the diffractometer. Graphite-monochromated Mo Kα radiation was used for the

X-ray diffraction study which was conducted on a computer-controlled four-circle Nicolet autodiffractometer. ω-Scan data collection was used with a scan range of $3.00 < 2\theta < 45.8°$. Other details of the data collection and refinement are given in Table 1.

The structure was solved using direct methods with the Siemens SHELXTL-Plus software package as modified at Crystalytics Company. Intensity data were corrected empirically for absorption effects by using ψ scans for seven reflections and were then reduced to relative squared amplitudes, F_o^2, by means of standard Lorentz and polarization corrections. Six standard reflections exhibited no significant loss of intensity throughout the course of data collection, and therefore no time-dependent intensity corrections were necessary. Anomalous dispersion corrections were applied to all non-hydrogen atoms in the anion.

Terminal methyl group carbon atom C_{22} on the bridging ethanethiol ligand was found to be disordered across the mirror plane at $z = \frac{1}{4}$ in the unit cell and was refined with an occupancy factor of 0.5 in each of the disordered positions. Hydrogen atom positions were not refined.

All atoms were refined with anisotropic thermal parameters using counter-weighted full matrix least-squares techniques. The refinement converged with final residuals of $R = 0.040$ and $R_w = 0.053$ and a goodness-of-fit indicator equal to 1.22. No peaks above the background noise level of 0.69 $e^-/Å^3$ remained in the final difference Fourier map.

Solution and refinement of the structure of $(Et_4N)_3[Mo_2Fe_7Se_8(SEt)_6(SC_6H_4Cl)_6]$

Crystals of $(Et_4N)_3[Mo_2Fe_7Se_8(SEt)_6(SC_6H_4Cl)_6]$ were grown by vapor diffusion of ether into an acetonitrile solution of the complex at room temperature. A black rectangular parallelepiped of approximate dimensions $0.10 \times 0.48 \times 0.95$ mm was mounted under a nitrogen atmosphere inside a glass capillary with a drop of mother liquor and with its longest edge nearly parallel to the phi axis of the diffractometer. Diffraction data was collected on a computer-controlled four-circle Nicolet autodiffractometer using graphite monochromated Mo Kα radiation. A total of 10,187 independent reflections were collected with full ω-scans (0.90° wide) and a range of $3.00 < 2\theta < 50.7°$. Other data collection and refinement parameters are listed in Table 1.

The structure was solved using direct methods with the Siemens SHELXTL-Plus software package as modified at Crystalytics Company. Intensity data were corrected for absorption effects by a numerical absorption correction using a Gaussian grid and produced a range of transmission factors of 0.153–0.667. Standard Lorentz and polarization corrections were applied and the data was reduced to relative squared amplitudes F_o^2. Six standard reflections exhibited no significant loss of intensity throughout the course of data collection, and therefore no time-dependent intensity corrections were necessary. Anomalous dispersion corrections were applied to all non-hydrogen atoms in the anion.

All atoms refined normally except for one of the cations, which appears to be statistically disordered with two possible orientations about the crystallographic inversion center at $(\frac{1}{2},0,0)$ in the unit cell. The carbon atoms of the terminal methyl groups for both orientations appear to occupy nearly the same positions in the lattice which are probably dictated by packing considerations. The methylene groups of each alkyl arm on cation no. 2 have two alternate (disordered) orientations in the lattice (see also 'Supplementary material').

The final structural model was refined with all non-hydrogen atoms having anisotropic thermal parameters and all locatable hydrogen atoms with isotropic thermal parameters. The phenyl ring hydrogen atoms and methylene hydrogens of the anion and of cation 1 were fixed at idealized sp^2- or sp^3-hybridized positions with a C–H bond length of 0.96 Å. The methyl group hydrogen atoms of the anion and cations were omitted from the structural model. The counter-weighted full-matrix least-squares refinement converged with final residuals of $R = 0.052$ and $R_w = 0.070$, and a goodness-of-fit indicator of 1.50.

Results and discussion

Synthesis

We have modified the synthetic procedure of O'Neal and Kolis [9a] for the preparation of MSe_4^{2-}. First, rather than producing the requisite binary selenide, K_2Se_3 from a liquid ammonia reaction system, we have prepared it by direct reaction of the elements under vacuum in sealed quartz tubes. This classical solid state synthetic route to binary selenides is simple and direct, but caution must be exercised due to the relatively violent nature of the highly exothermic reaction. Thick-walled quartz tubing must be used and care taken during the sealing process to prevent formation of weak, thin-walled areas. The reaction ensues very rapidly at 63 °C, which is the melting point of potassium metal. Further heating to 350 °C ensures production of a homogeneous product. The second modification employed in the $MoSe_4^{2-}$ preparation was the substitution of a flowing argon reaction system for the closed, 'static

TABLE 1. Summary of crystallographic parameters

Formula	$((C_2H_5)_4N)_3[Mo_2Fe_6Se_8(SC_2H_5)_9]$	$((C_2H_5)_4N)_3[Mo_2Fe_7Se_8(SC_2H_5)_6(SC_6H_4Cl)_6]$
Molecular wt	2100.0	2833.6
a (Å)	17.453(3)	11.401(2)
b (Å)	17.453(3)	12.697(2)
c (Å)	16.575(2)	19.897(3)
α (°)	90.00	87.91(1)
β (°)	90.00	74.93(1)
γ (°)	120.00	89.14(2)
Crystal system	hexagonal	triclinic
V (Å^3)	4375(1)	2779.4(9)
Z	2	1
D_{calc} (g/cm^3)	1.595	1.693
D_{obs} (g/cm^3)	1.61	1.69
Space group	$P6_3/m$	$P\bar{1}$
Crystal dimensions (mm)	0.27×0.27×0.82	0.10×0.48×0.95
Radiation	Mo Kα (λ=0.71073 Å)	Mo Kα (λ=0.71073 Å)
Linear absorption coefficient (mm^{-1})	4.47	3.86
Scan speed (°/min)	4 ($3.0<2\theta<39.7$) 2 ($39.7<2\theta<45.8$)	6 ($3.0<2\theta<43.0$) 4 ($43.0<2\theta<50.7$)
Scan range (°)	$3.0<2\theta<45.8$	$3.0<2\theta<50.7$
Data collected	2095	10187
Unique data, ($I_0>3\sigma(I_0)$)	1159	6052
No. variables	122	536
Goodness of fit	1.22	1.60
R (%)	4.0	5.2
R_w (%)	5.3	7.0

vacuum' system previously described [9a]. This modification avoids the potentially hazardous pressure build-up from the carbon monoxide co-product (eqn. (1)).

$$K_2Se_3 + M(CO)_6 + 2[(R_4N)Br] \longrightarrow (R_4N)_2[MSe_4] + 6CO + 2KBr \quad (1)$$

Heptane is added to the solvent mixture and continuously condenses carrying along any of the $M(CO)_6$ that has sublimed onto the condenser. Finally, analytically pure products were obtained by recrystallization from acetonitrile/ether with KBr being the primary impurity. With these modifications, large batches of analytically pure $(Et_4N)_2[MSe_4]$ (M = Mo, W) have been repeatedly produced.

The anaerobic reaction system (eqn. (2))

$$[MSe_4]^{2-} + 3\text{–}3.5FeCl_3 + 9\text{–}12NaSEt \longrightarrow \begin{matrix} [M_2Fe_6Se_8(SEt)_9]^{3-} & \mathbf{1} \\ [M_2Fe_7Se_8(SEt)_{12}]^{3-} & \mathbf{3} \\ [W_2Fe_7Se_8(SEt)_{12}]^{4-} & \mathbf{4} \end{matrix} \quad (2)$$

where M = Mo, W, is based upon that developed by Holm [1a], and Christou *et al.* [3] for the analogous sulfur complexes. Variation of the reaction stoichiometries and solvents lead to preferential production of a single cluster type, though fractional crystallization is required to obtain analytically pure products. ^{1}H NMR spectroscopy proved to be the most informative method for monitoring product purity. In this regard, impure samples of type **1** clusters were found to contain paramagnetic impurities that likely are $[Mo_2Fe_6Se_8S(SEt)_8]^{3-}$; but it is also possible that $[Mo_2Fe_6Se_9(SEt)_8]^{3-}$ may have been produced. No extended efforts were made to isolate this type of double-cubane species. A single-crystal structure determination of a type **1** cluster with M = Mo was undertaken and the results are presented below.

An investigation into the substitutional lability of the thiolate ligands in these double-cubane anions was undertaken as outlined in reactions (3) and (4):

$$[Mo_2Fe_7Se_8(SEt)_{12}]^{3-} + 6HSAr \longrightarrow [M_2Fe_7Se_8(SEt)_6(SAr)_6]^{3-} \quad (3)$$

$$[Mo_2Fe_7Se_8(SEt)_{12}]^{3-} + 6 \text{ acetyl chloride} \longrightarrow [M_2Fe_7Se_8(SEt)_6Cl_6]^{3-} \quad (4)$$

where M = Mo, W. As previously observed by Holm [1a], only the terminal thiolate ligands undergo ex-

change, leaving the bridging thiolate ligands intact. Such substitutions proved to be useful in confirming NMR assignments and also in obtaining structural characterization of the type 3 cluster, with M = Mo, which will be discussed in detail below. Overall, the tetraselenometallate dianions reacted very similarly to their tetrathiometallate analogs with the production of the corresponding selenium double-cubanes in comparable yield and purity. Significantly, all the complexes contain the full stoichiometric amount of four seleniums per cubane unit, indicating that MSe_4^{2-} can effectively deliver all four selenium atoms in the assembly process even though one is no longer covalently bound to M.

Structure of $(Et_4N)_3[Mo_2Fe_7Se_8(SEt)_6(SC_6H_4Cl)_6]$

$(Et_4N)_3[Mo_2Fe_7Se_8(SEt)_6(SC_6H_4Cl)_6]$ crystallizes in the triclinic space group $P\bar{1}$ (No. 2) with $a = 11.401(2)$, $b = 12.697(2)$, $c = 19.897(3)$ Å, $\alpha = 87.91(1)$, $\beta = 74.93(1)$, $\gamma = 89.14(2)°$ and $Z = 1$. The cation and ligand bond distances and angles are unexceptional and will not be considered further. The structure of the anion is shown in Fig. 1. Metrical data are tabulated in Tables 2 and 3. The central Fe atom is located at a crystallographic inversion center and is in an imperfect distorted trigonal-antiprismatic environment coordinated to six μ_2-S atoms from ethanethiolate ligands. The mean Fe–S bond distance of 2.306(8) Å is suggestive of a low-spin Fe(III) and is nearly identical to the mean Fe–S distance of 2.309(9) Å that was observed in the most similar sulfur analog $(Me_3NCH_2Ph)_3[Mo_2Fe_7S_8(SEt)_{12}]$ [17]. It should be noted that the exact sulfide analog of this selenide double-cubane has not been structurally characterized so that all subsequent references to the 'sulfur analog' actually refer to the most similar sulfur analog: $(Me_3NCH_2Ph)_3[Mo_2Fe_7S_8(SEt)_{12}]$. The Mo···$Fe_4$ distance of 3.316(1) Å and the Mo···Mo distance of 6.632(2) Å are nearly identical to that observed in the sulfur analog: 3.319(1) and 6.638(2) Å, respectively. This provides further evidence of the near equivalence of the bridging portions in these two structures.

The two $MoFe_3Se_4(SR)_3$ cubane-like subclusters differ systematically from their sulfur analogs in a manner consistent with the substitution of the larger selenide for the sulfide. The mean Mo–Se bond distance of 2.490(4) Å and the mean Fe–Se bond distance of 2.388(8) Å are 4% longer than the mean Mo–S (2.357(7) Å) and Fe–S (2.270(12) Å) bond distances in $(Me_3NCH_2Ph)_3[Mo_2Fe_7S_8(SEt)_{12}]$ [17]. This is a rather small increase in bond distance in light of the 8% larger ionic radii of Se^{2-} relative to S^{2-} [18]. Despite this 4% bond length increase upon selenium substitution, only a 1% increase in the mean Mo···Fe distance across the face of the cube is observed: Se, 2.767(12) Å; S, 2.730(14) Å. A comparable change in the mean Fe···Fe distances in the remaining cubane faces was found: Se, 2.750(14) Å; S, 2.730(14) Å. As a consequence of these nearly identical intermetallic distances and incorporation of the larger selenide ions, the angles formed by the bridging selenium atoms are significantly more acute. In the sulfur analog the mean Mo–Fe–S angle is 72.4°; whereas, in the selenium analog it is diminished to 69.3°. This observation

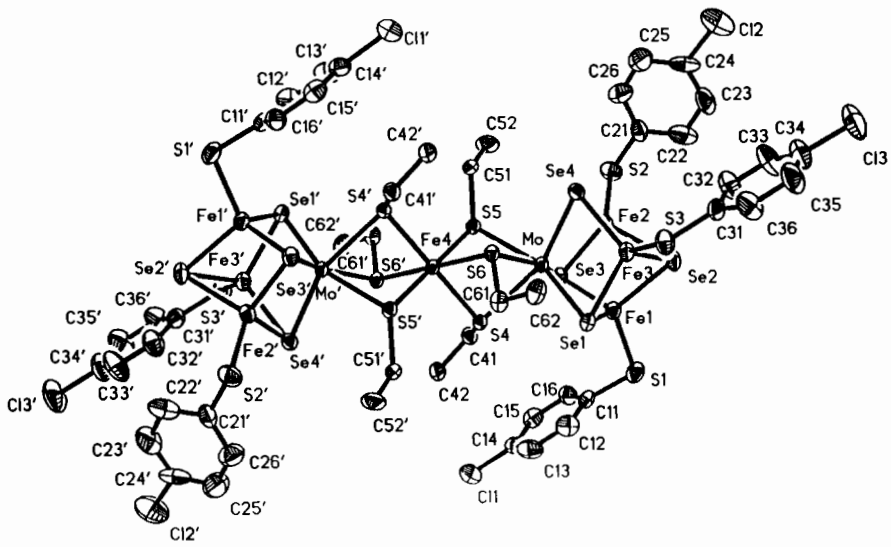

Fig. 1. Structure of $[Mo_2Fe_7Se_8(SEt)_6(SC_6H_4Cl)_6]^{3-}$ showing the labeling scheme and 30% probability ellipsoids.

TABLE 2. Interatomic distances (Å) and e.s.d.s of the anion $[Mo_2Fe_7Se_8(SEt)_6(SC_6H_4Cl)_6]^{3-}$

Mo···Mo	6.632(2)	Fe1–Se1	2.372(2)
Mo···Fe1	2.808(2)	Fe1–Se2	2.369(2)
Mo···Fe2	2.747(2)	Fe1–Se3	2.376(2)
Mo···Fe3	2.747(2)	Fe2–Se2	2.436(2)
Mo···Fe4	3.316(1)	Fe2–Se3	2.364(2)
Fe1···Fe2	2.755(2)	Fe2–Se4	2.385(2)
Fe1···Fe3	2.767(2)	Fe3–Se1	2.371(2)
Fe2···Fe3	2.729(2)	Fe3–Se2	2.433(2)
Mo–Se1	2.490(1)	Fe3–Se4	2.389(2)
Mo–Se3	2.499(1)	Fe1–S1	2.242(4)
Mo–Se4	2.482(1)	Fe2–S2	2.269(3)
Mo–S4	2.550(2)	Fe3–S3	2.278(3)
Mo–S5	2.546(3)	Fe4–S4	2.324(3)
Mo–S6	2.566(3)	Fe4–S5	2.281(2)
Se1···Se2	3.780(3)	Fe4–S6	2.314(2)
Se1···Se3	3.910(1)	Se2···Se3	3.793(2)
Se1···Se4	3.956(2)	Se2···Se4	3.881(2)
		Se3···Se4	3.949(1)

TABLE 3. Interatomic angles (°) and e.s.d.s for the anion $[Mo_2Fe_7Se_8(SEt)_6(SC_6H_4Cl)_6]^{3-}$

Se1–Mo–Se3	103.2(1)	Se1–Mo–Se4	105.4(1)
Se3–Mo–Se4	104.9(1)	Se1–Mo–S4	86.9(1)
Se1–Mo–S5	158.0(1)	Se1–Mo–S6	90.4(1)
Se4–Mo–Se4	156.1(1)	S4–Mo–S5	73.2(1)
Se1–Fe1–Se2	105.8(1)	Se1–Fe1–Se3	110.9(1)
Se1–Fe1–S1	111.7(1)	Se2–Fe1–Se3	106.1(1)
S4–Fe4–S5	82.6(1)	S4–Fe4–S6	82.2(1)
S5–Fe4–S6	85.4(1)	Mo–S4–Fe4	85.6(1)
Mo–S6–Fe4	85.4(1)	Mo–S5–Fe4	86.6(1)
Mo–Se1–Fe3	68.8(1)	Mo–Se1–Fe1	70.5(1)

suggests that the stability of the MFe_3X_4 cubane subcluster is enhanced by the maintenance of optimum metal-to-metal distances within the cube, even at the expense of weaker metal chalcogenide bonding due to the more acute bridging angles. This unusual structural perturbation has been observed in the related $Fe_4X_4^{2-}$ thiocubanes as well [13a], and appears to be a characteristic feature of such cubane and now double-cubane complexes. The mean Fe–Se bond length of 2.388(8) Å is close to that observed in the related seleno-cubane $(Et_4N)_2[Fe_4Se_4(SC_6H_5)_4]$ molecule: 2.387(2) Å [13a]. The Mo–Se bond length of 2.490(4) Å is considerably longer than the 2.293(1) Å bond length found in the $MoSe_4^{2-}$ starting material [9a] and is consistent with the reduction of the Mo from Mo(VI) to Mo(III) with a concomitant increase in coordination number and reduction of the Mo–Se bond order from two to one. For example, in $MoSe(Se_4)_2^{2-}$ the mean Mo–Se single bond length is 2.469(2) Å [9a]; in $MoO(Se_4)_2^{2-}$, 2.49(2) Å [9b]; and in $Cp_2Mo_2SeO_3$ it is 2.431(2) Å [19]. No statistically significant variation in Fe–Se bond lengths is observed in accord with a delocalized model for the formally $Fe^{+2.67}$ ions, as opposed to a localized Fe^{+3} and Fe^{+2} ion model. The mean Fe–S (terminal) bond distance of 2.263(4) Å agrees closely with that found in $(Et_4N)_3[Mo_2Fe_3S_8(SC_6H_5)_{12}]$: 2.256(4) Å, indicating that no significant change in the formal oxidation state of the subcluster Fe atoms has occurred, and that all three Fe are equivalent.

As has been noted in the sulfide analogs, these $MoFe_3Se_4$ subclusters are trigonally distorted from cubic symmetry by compression of the Se_4 tetrahedra along the idealized three-fold axis which passes through Mo and Se2 [17]. The Se···Se distances perpendicular to this axis average 3.938(7) Å, whereas the mean value of the three remaining Se···Se distances is 3.818(8) Å. The subcluster body diagonal planes are nearly perfect; for example, the mean deviation from the plane defined by Mo–Se1–Se2–Fe2 is 0.0021 Å (see also 'Supplementary material'). Overall, ignoring the *p*-chlorothiophenol ligands, the subcluster symmetry closely conforms to C_{3v}.

Structure of $(Et_4N)_3[Mo_2Fe_6Se_8(SEt)_9]$

$(Et_4N)_3[Mo_2Fe_6Se_8(SEt)_9]$ crystallizes in the hexagonal space group $P6_3/m$ (No. 176) with $a = 17.453(3)$, $c = 16.575(2)$ Å and $Z = 2$. The cations lie on the mirror planes at $z = \frac{1}{4}, \frac{3}{4}$, are well separated from the anions, and contain no exceptional bond distances or angles. The structure of the anion is shown in Fig. 2. The anion consists of two $MoFe_3Se_4(SEt)_3$ subclusters identical to those described above, but in this structure they are bridged by three μ_2-ethanethiolate ligands rather than the $Fe(SEt)_6$ group. The three bridging sulfur atoms lie at $z = \frac{1}{4}$ on the mirror plane which imposes a strict equivalence upon the two subclusters. In addition, a crystallo-

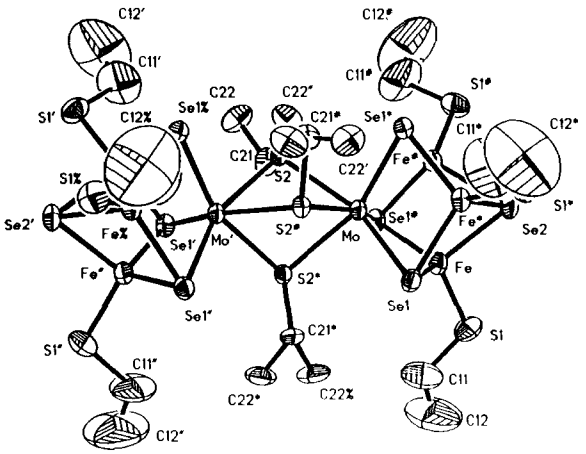

Fig. 2. Structure of $[Mo_2Fe_6Se_8(SEt)_9]^{3-}$ showing the atom labeling scheme and 30% probability ellipsoids. Hydrogen atoms are omitted for clarity.

graphic three-fold axis at $x=\frac{1}{3}$, $y=\frac{2}{3}$ coincides with the Se2–Mo–Mo′–Se2′ anion vector. Metrical data are tabulated in Tables 4 and 5.

The subcluster structure in these anions is nearly identical with that discussed in the previous complex. The mean Mo–Se bond length of 2.479(1) Å and the mean Fe–Se bond length of 2.378(2) Å are slightly shorter than the respective bond lengths in the preceding structure: 2.490(4) and 2.388(8) Å. This difference is possibly due to less electron donation into the subcluster by the terminal aromatic thiolate ligands relative to ethanethiolate; and may be influenced by the steric and electronic effects of the different inter-subcluster bridging groups. The Mo–Se–Fe angles again are significantly more acute (70.1(1)°) relative to the analogous sulfide complex (72.5(2)°) [20]. The mean cube face diagonal Mo···Fe distance of 2.793(2) Å is longer than that found in the previous structure: 2.767(12) Å; however, the mean Fe···Fe distance, 2.746(3) Å is slightly shorter: 2.750(15) Å. Both are slightly longer than the mean Mo···Fe and Fe···Fe distances in the analogous sulfide complex: 2.723(2) and 2.687(3) Å, respectively. Again, the incorporation of the larger selenide ion into the double-cubane structure has a minimal impact upon the intracluster metal-to-metal separations, although it leads to significant changes in the bridging chalcogenide bond angles. The distortion from cubic symmetry is again evident in these subclusters, with the Se···Se distances perpendicular to the trigonal axis being 3.910(1) Å whereas the remaining Se···Se distance is 3.822(2) Å indicating that the cube has been compressed. The subcluster body diagonal planes are nearly perfect; for example, the mean deviation from the plane defined by Mo–Se1–Se2–Fe# is 0.001 Å. The remaining body diagonal least-squares planes are included in the supplementary material. The local subcluster symmetry closely approximates C_{3v}. Overall, the subcluster structure is very similar to that of the analogous sulfur complex with differences explicable in terms of the larger radii of selenide relative to sulfide. The small differences between the subclusters compared to the previous structure likely arise from the substitution of aryl thiolates with alkyl thiolates on the subclusters, as well as from electronic and steric effects of the different subcluster bridging groups.

TABLE 4. Interatomic distances (Å) and e.s.d.s of the anion $[Mo_2Fe_6Se_8(SEt)_9]^{3-}$

Mo···Mo′	3.714(3)	Fe–S1	2.231(6)
Mo···Fe	2.793(2)	Fe–Se2	2.405(2)
Fe···Fe*	2.746(3)	Fe–Se1	2.381(2)
Mo···Se2	4.108(4)	Fe*–Se1	2.376(2)
Mo–Se1	2.479(1)	Se(1)···Se1*	3.910(1)
Mo–S2	2.581(3)	Se(1)···Se2	3.822(2)

TABLE 5. Interatomic angles (°) and e.s.d.s for the anion $[Mo_2Fe_6Se_8(SEt)_9]^{3-}$

Se1–Mo–S2	158.3(1)	Se1–Fe–Se1#	110.5(1)
Se1–Mo–Se1*	104.1(1)	Se1–Fe–Se2	106.0(1)
Se1–Mo–Fe	53.3(1)	Se1–Fe–S1	114.1(1)
S2–Mo–S2*	74.0(1)	Se2–Fe–S1	104.0(1)
S2–Mo–Se1*	87.3(1)	S1–Fe–Se1#	115.0(1)
S2–Mo–Se1#	90.6(1)	Mo–S2–Mo′	92.0(2)
Mo–Se1–Fe	70.1(1)	Fe–Se2–Fe*	69.6(1)

The two subclusters are bridged by three μ_2-S ethanethiolates, the sulfur atoms and methylene carbons of which lie in the mirror plane. The methyl groups of the ethanethiolates are disordered about the mirror plane with statistically expected equal occupancy of the two orientations. The Mo–SEt (bridging) bond length of 2.581(3) Å is slightly longer than in $(Et_4N)_3[Mo_2Fe_7Se_8(SEt)_6(SC_6H_4Cl)_6]$: 2.567(4) Å. The Mo···Mo distance of 3.714(3) Å is slightly longer than that observed in $(Et_4N)_3[Mo_2Fe_6S_8(SC_6H_5)_9]$ (3.685(3) Å) or in $(Et_4N)_3[Mo_2Fe_6S_8(SEt)_9]$ (3.668(4) Å) [20].

Electronic spectra

The electronic absorption spectra of the selenium double-cubane complexes are all characterized by a resolved band at 350–425 (M = Mo) or 385–394 (M = W) nm in acetonitrile. A second, typically unresolved shoulder is found at 259–284 (M = Mo) or 259–275 (M = W) nm, respectively. The characteristic shapes of these spectra are similar to those observed in the analogous sulfide double-cubanes but are red-shifted by 3–10 nm [21]. Absorption maxima and extinction coefficients are given in Table 6 along with those of several sulfur analogs. The band shift is consistent with the bands' origins as RS → core ligand-to-metal charge transfer bands. The less electronegative selenium atoms stabilize the core LUMO level relative to that in the sulfur analogs. More dramatic red shifts of 20–30 nm occurs upon substitution of the less electron-donating terminal groups such as aromatic thiolates in $[Mo_2Fe_7Se_8(SEt)_{12}]^{2-}$. Excitation from energy levels in these ligands which are stabilized relative to the ethanethiol energy levels results in the lower energy transitions observed. This same effect has been noted in the sulfur analogs [21].

^{1}H NMR spectroscopy

Assignment of ^{1}H NMR resonances was primarily deduced by comparison with the ^{1}H NMR of the sulfur analogs [22]. Displacement of terminal

TABLE 6. UV–Vis spectral data for selenium double-cubane complexes

Complex	Absorption maxima (nm) ($10^{-3} \times \epsilon$ (M^{-1} cm^{-1}))[a]
$[Mo_2Fe_6Se_8(SEt)_9]^{3-}$	282(57.8), 395(34.5)
$[Mo_2Fe_6S_8(SEt)_9]^{3-}$[b]	277(58.2), 391(35.5)
$[W_2Fe_6Se_8(SEt)_9]^{3-}$	259(56.5), 387(34.4)
$[Mo_2Fe_7Se_8(SEt)_{12}]^{3-}$	283(74.2), 398(56.8)
$[Mo_2Fe_7S_8(SEt)_{12}]^{3-}$[b]	281(73.9), 394(56.4)
$[Mo_2Fe_7S_8(SEt)_6(SC_6H_5)_6]^{3-}$	284(sh,130.2), 350(sh,60.5), 425(sh,58.2)
$[Mo_2Fe_7Se_8(SEt)_6(SC_6H_4Cl)_6]^{3-}$	280(sh,128.6), 370(sh,60.2), 420(sh,57.9)
$[Mo_2Fe_7Se_8(SEt)_6Cl_6]^{3-}$	275(73.5), 360(sh,28.3)
$[W_2Fe_7Se_8(SEt)_{12}]^{3-}$	273(63.5), 398(47.2)
$[W_2Fe_7S_8(SEt)_{12}]^{3-}$[b]	266(64.8), 395(47.5)
$[W_2Fe_7Se_8(SEt)_{12}]^{4-}$	270(75.9), 385(48.7)
$[W_2Fe_7S_8(SEt)_{12}]^{4-}$[b]	257(76.5), 380(49.2)

[a]In acetonitrile. [b]Ref. 21b.

ethanethiolate groups with aryl thiolates and chloride anions in $[Mo_2Fe_7Se_8(SEt)_{12}]^{3-}$ provided confirmation of the assignment of bridging and terminal thiolate groups in these complexes. *In situ* titration of other double-cubane species with acetyl chloride or benzenethiol in NMR tubes was employed as a check upon assignments of bridging versus terminal ethanethiolate resonances. Previous work, as well as our own studies have shown that bridging ethanethiolate groups are inert to displacement by these reagents, whereas the terminal ethanethiolate groups undergo ready displacement [21b]. Methyl versus methylene assignments were usually evident from relative peak intensities. The isotropic shifts, $(\Delta H/H_0)_{iso}$, were calculated from the observed chemical shifts by subtracting the corresponding diamagnetic shift of the free ligand in CD_3CN: $(\Delta H/H_0)_{iso} = (\Delta H/H_0)_{obs} - (\Delta H/H_0)_{diam}$ [22]. These isotropic shifts are tabulated in Table 7 along with those of some corresponding sulfur analogs. Representative NMR of the selenium double-cubanes are presented in Figs. 3 and 4.

In general, the observed isotropic shifts are larger for the selenium double-cubanes relative to their sulfur analogs. The isotropic shifts in these types of complexes are thought to arise primarily from contact shift contributions, which are proportional to the magnetic susceptibility at a given temperature. The larger isotropic shifts in the selenium double-cubanes are consistent with their larger room temperature solution magnetic susceptibilities relative to their sulfur analogs. These room temperature solution magnetic susceptibilities (X_m) were determined by the Evans method in CH_3CN. For example, the isotropic shift of the terminal ligand methylene protons in $[Mo_2Fe_6Se_8(SEt)_9]^{3-}$ are observed at -59.5 ppm, whereas the same protons in the sulfur analog are found at -53.2 ppm. The larger isotropic shift in the selenium complex is consistent with its larger magnetic moment ($\mu_{eff} = 2.828 X_m T$) of 6.01 μ_B relative to the sulfur complex: 5.73 μ_B [21b]. These same methylene protons in $[W_2Fe_6Se_8(SEt)_9]^{3-}$ are observed at -52.9 ppm and its room temperature solution magnetic moment is 5.65 μ_B [21a]. Again, the smaller isotropic shift correlates with the smaller magnetic moment. This same relationship is observed in the case of the type 3 cubanes as well. The larger

TABLE 7. ^1H isotropic shifts in CD_3CN at 23 °C

Complex	$(\Delta H/H_0)_{iso}$ (ppm)			
	terminal		bridging	
	CH_2	CH_3	CH_2	CH_3
$[Mo_2Fe_6Se_8(SEt)_9]^{3-}$	−59.5	−4.62	−15.8	+1.95
$[Mo_2Fe_6S_8(SEt)_9]^{3-}$[a]	−53.2	−3.48	−15.0	
$[W_2Fe_6Se_8(SEt)_9]^{3-}$	−52.9	−3.49	−12.7	+1.87
$[W_2Fe_6S_8(SEt)_9]^{3-}$[b]	−51.4	−3.22	−9.89	
$[Mo_2Fe_7Se_8(SEt)_{12}]^{3-}$	−55.5	−3.07	−21.4, −12.6	+1.07
$[Mo_2Fe_7S_8(SEt)_{12}]^{3-}$[a]	−53.2	−3.23	−21.9, −15.0	+0.46
$[W_2Fe_7Se_8(SEt)_{12}]^{3-}$	−53.9	−3.02	−12.2, −5.00	+0.83
$[W_2Fe_7S_8(SEt)_{12}]^{3-}$[a]	−51.6	−3.01	−13.3, −7.03	+0.78
$[Mo_2Fe_7Se_8(SEt)_6(SC_6H_4Cl)_6]^{3-}$	[c]	[c]	−22.4, −8.81	+0.59
$[Mo_2Fe_7Se_8(SEt)_6(Cl_6)]^{3-}$			−34.9, −21.7	+3.17
$[Mo_2Fe_7Se_8(SEt)_6(SC_6H_5)_6]^{3-}$	[d]	[d]	−21.5, −8.21	+0.52
$[W_2Fe_7Se_8(SEt)_{12}]^{4-}$	−59.0	−7.75	−87.5[e]	+28.2
$[W_2Fe_7S_8(SEt)_{12}]^{4-}$[a]	−54.9	−7.49	−82.0[e]	+22.7

[a]Ref. 21b. [b]Ref. 21a. [c]*ortho*-, +10.72; *meta*, −6.41 ppm. [d]*ortho*-, +10.1; *meta* −6.60; *para*, +10.6 ppm. [e]Exchange-averaged signal.

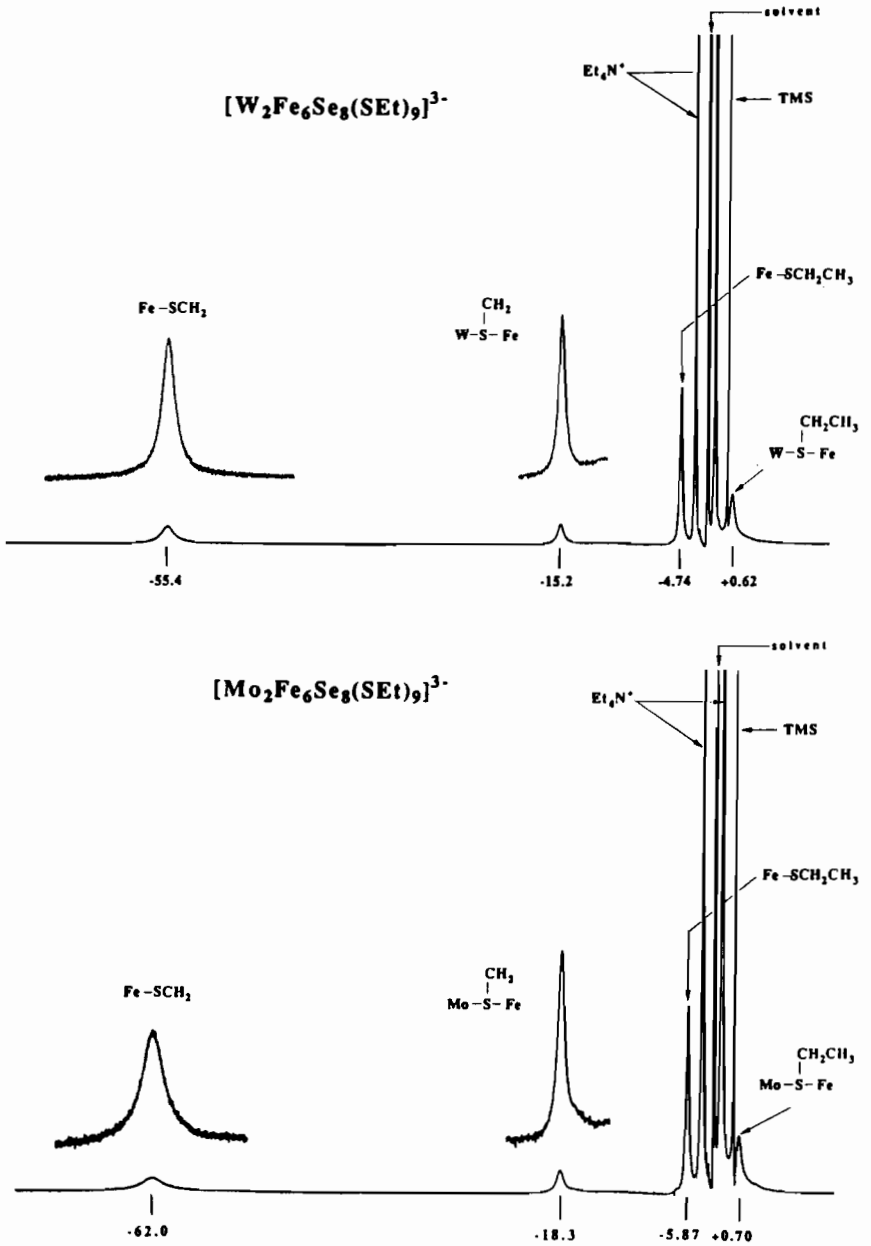

Fig. 3. ^{1}H FT-NMR spectra (360 MHz) of $(Et_4N)_3[M_2Fe_6Se_8(SEt)_9]$ (M = Mo, W) in CD_3CN at 22 °C. Signal assignments are as indicated.

magnetic moments observed in the selenium double-cubanes indicate that the larger metal-to-metal separations which result from incorporation of selenium in the thiocubane subclusters lead to a smaller antiferromagnetic coupling between the metals. This is the origin of the larger room temperature magnetic susceptibility. The opposing influence of selenium's greater covalency, which should increase antiferromagnetic coupling between the metals appears to be less influential. Similar behavior has been reported for the paramagnetic $Fe_4X_4(SR)_4^{2-/3-}$ system, where X = S, Se [22].

Slightly larger isotropic shifts are noted for the Mo-type clusters relative to the W analogs and had been noted in the sulfide double-cubanes [21]. This trend was attributed to greater incipient metal-to-metal bond formation in the W clusters which would reduce the magnetic moments on the cluster and thereby diminish the contact shift contribution to the isotropic shifts [21a]. Our solution magnetic data

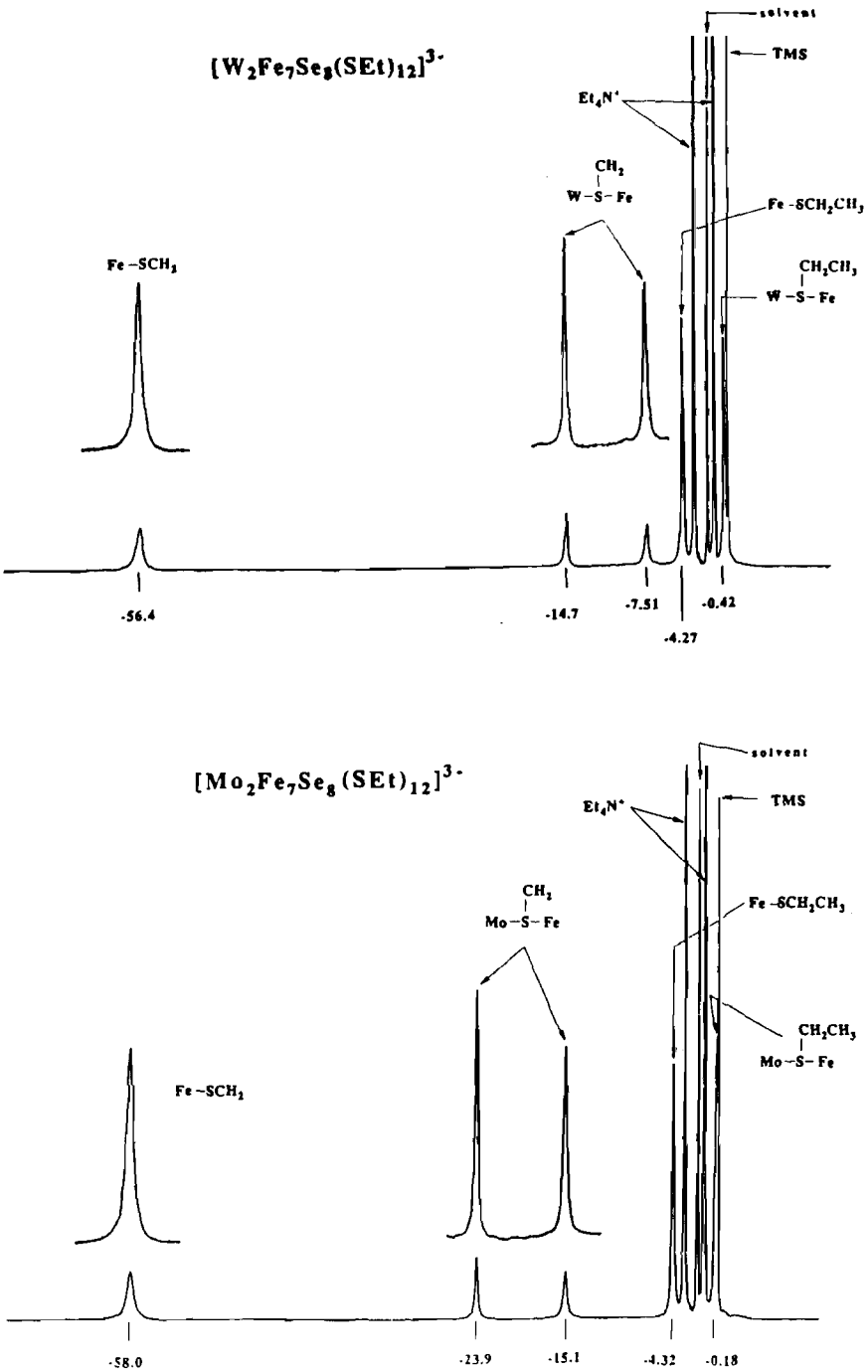

Fig. 4. ^{1}H FT-NMR spectra (360 MHz) of $(Et_4N)_3[M_2Fe_7Se_8(SEt)_{12}]$ (M = Mo, W) in CD_3CN at 22 °C. Signal assignments are as indicated.

indicate that the W-selenium double-cubanes do have slightly smaller magnetic susceptibilities at room temperature relative to their Mo analogs. In the case of the reduced double-cubane, $[W_2Fe_7Se_8(SEt)_{12}]^{4-}$, the largest isotropic shift is found for the methylene protons of the bridging ligands, unlike the previously discussed complexes in which the largest shifts are observed for the terminal methylene protons. This is likely due to the proximity of the methylene groups to the bridging Fe which is now a high-spin Fe(II) [21b]. The large isotropic shifts of these protons (−87.5 ppm) is again

consistent with the molecules' large magnetic moment: 10.3 μ_B.

Previous workers have concluded that the isotropic shifts of terminal thiolate groups in sulfur double-cubane complexes arise predominantly from contact terms with little or no contribution from dipolar interactions. We find this to be true in the selenium double-cubanes as well. Figure 5 illustrates the near-linear proportionality of the terminal ligand methylene isotropic shifts and the solution magnetic moments as a function of temperature for $[Mo_2Fe_6Se_8(SEt)_9]^{3-}$. The negative temperature dependence of the methylene protons' isotropic shifts over the temperature range of -40 to $+60$ °C is illustrated in Fig. 6 for several of the selenium double-cubanes. The alternating sign of the aromatic proton shifts in $[Mo_2Fe_7Se_8(SEt)_6(SC_6H_5)_6]^{3-}$, with the *ortho*- and *para*-H shifted upfield and the *meta*-H shifted downfield is indicative of contact shifts via a π delocalization mechanism [23]. In addition, the shifts

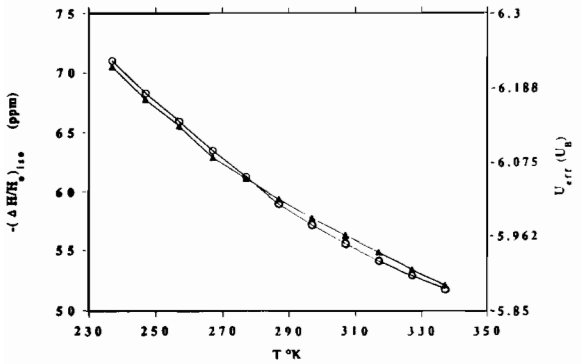

Fig. 5. Temperature dependence of the terminal SCH_2 isotropic shift of $(Et_4N)_3[Mo_2Fe_6Se_8(SEt)_9]$ in CD_3CN (△) with the solution magnetic moment (○). The scales were arbitrarily chosen such that $(\Delta H/H_0)_{iso}$ and X_m coincide at 277 K.

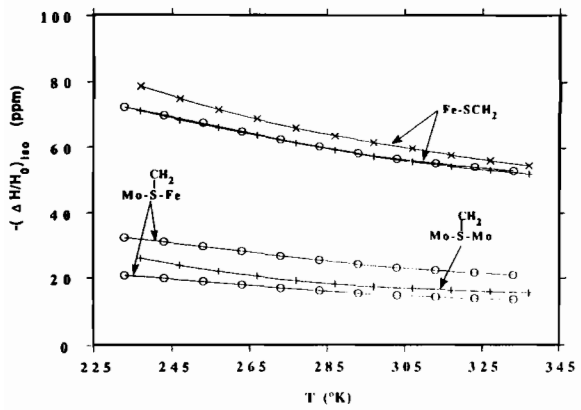

Fig. 6. Temperature dependence of terminal and bridging SCH_2 isotropic shifts in CD_3CN solution: ×, $[W_2Fe_7Se_8(SEt)_{12}]^{4-}$; ○, $[Mo_2Fe_7Se_8(SEt)_{12}]^{3-}$; +, $[Mo_2Fe_6Se_8(SEt)_9]^{3-}$.

are not attenuated by distance (*meta*-H = -6.60 ppm, *para*-H = $+10.6$ ppm) which would be expected if the dominant interaction were dipolar in origin. Taken together, these observations lead to the conclusion that the dominant isotropic shift interaction of the terminal thiolate ligands in the selenium double-cubanes is predominantly contact in origin.

Electrochemistry

Cyclic voltammograms of representative selenium double-cubane complexes obtained in acetonitrile at ambient temperature are presented in Fig. 7. Irreversible oxidation processes at potentials >0.50 V versus SCE will not be discussed. Strict electrochemical reversibility as defined by a 59 mV peak separation for a 1 e^- process was not observed for these complexes with typical separations between the cathodic and anodic waves being 60–80 mV at 100 mV/s scan rates. However, effective electrochemical reversibility can be inferred from ratios of cathodic to anodic currents ($i_{p,c}/i_{p,a}$) and for waves described as 'reversible' in this paper this ratio approaches unity. The reversible Fe^{2+}/Fe^{3+} couple in ferrocene was observed at +0.394 V versus SCE in our experimental arrangement with a peak-to-peak separation of 63 mV. The half-wave potentials of reversible electrochemical processes are tabulated in Table 8, along with those of several analogous sulfur double-cubane complexes for comparison.

The cyclic voltammograms of cluster type **1** are presented in Fig. 7 and clearly indicate two well-resolved reversible electrochemical processes. Electron transfer series 4 has been postulated for the analogous sulfur double-cubanes [21] and is likely applicable as well here:

$$[M_2Fe_6X_8(SEt)_9]^{3-} \rightleftharpoons$$

$$[M_2Fe_6X_8(SEt)_9]^{4-} \rightleftharpoons [M_2Fe_6X_8(SEt)_9]^{5-} \quad (4)$$

where M = Mo, W; X = S, Se. It is assumed that the two processes represent stepwise reduction of the two subclusters in the complex. As noted in the sulfur analogs, and as is generally observed, it is significantly easier to reduce the molybdenum containing subclusters relative to their tungsten analogs. Substitution of selenium for sulfur in these subclusters, however, has a surprisingly small effect upon the reduction potentials as can be seen in Table 8. The 10–20 mV differences are within the experimental uncertainty of such measurements. The observation that replacement of eight sulfide ions with eight selenide ions has nearly no impact upon the reduction potentials is quite surprising. Recent work by Rauchfuss and coworkers, in contrast, has shown ≈100 mV differences in redox potentials upon substitution of Se for S in coordination complexes containing

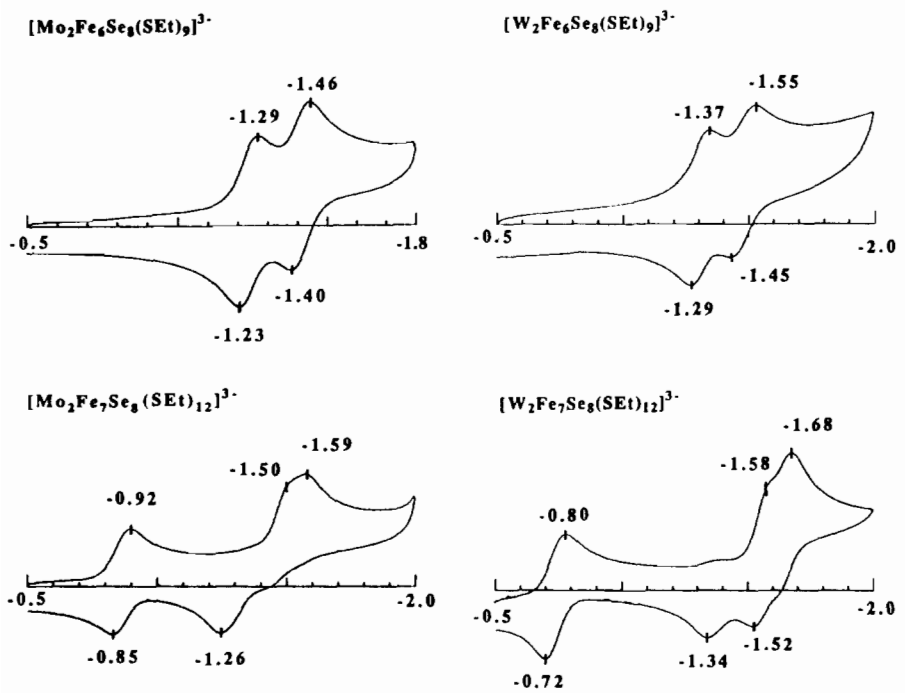

Fig. 7. Cyclic Voltammograms of $[M_2Fe_6Se_8(SEt)_9]^{3-}$ and $[M_2Fe_7Se_8(SEt)_{12}]^{3-}$ (M=Mo, W) in acetonitrile at 25 °C and a scan rate of 100 mV/s. Peak potentials vs. SCE are indicated.

TABLE 8. Electrochemical parameters of double-cubane complexes[a]

Complex	$E_{1/2}$ (reversible) (V)[b]
$[Mo_2Fe_6Se_8(SEt)_9]^{3-}$	−1.26, −1.43
$[Mo_2Fe_6S_8(SEt)_9]^{3-}$	−1.28, −1.47[c]
$[W_2Fe_6Se_8(SEt)_9]^{3-}$	−1.33, −1.50
$[Mo_2Fe_7Se_8(SEt)_{12}]^{3-}$	−0.88
$[Mo_2Fe_7S_8(SEt)_{12}]^{3-}$	−0.89[c]
$[W_2Fe_7Se_8(SEt)_{12}]^{3-}$	−0.76
$[W_2Fe_7S_8(SEt)_{12}]^{3-}$	−0.76[c]
$[Mo_2Fe_7Se_8(SEt)_6(SC_6H_5)_6]^{3-}$	−0.73
$[Mo_2Fe_7Se_8(SEt)_6(SC_6H_4Cl)_6]^{3-}$	−0.72
$[Mo_2Fe_7Se_8(SEt)_6Cl_6]^{3-}$	−0.65

[a]All redox potentials were measured in CH_3CN, 0.1 M Bu_4NPF_6 (scan rate = 100 mV/s) vs. SCE; glassy carbon working electrode. [b]$E_{1/2} = 1/2(E_c + E_a)$. [c]Ref. 21b.

MX_4^{2-} [10]. It is possible that the greater electronegativity of selenium is being negated by its poorer orbital overlap with the cubane metals due to its unusually acute bridging angles.

The cyclic voltammogram of cluster type **3** is illustrated in Fig. 7 and exhibits two well-separated reduction processes. The same behavior has been observed in the sulfur analogs [21]. The initial reversible reduction corresponds to reduction of the unique bridging iron located at the inversion center of the molecule. Structural characterization of such $1e^-$ reduced complexes in the sulfide case has confirmed that the iron has been reduced from a low spin Fe(III) to a high spin Fe(II) [17]. The second reduction process is actually a composite of two stepwise reductions of single subclusters within the molecule. Due to the larger subcluster distance, these two processes interact less than in the type **1** complexes, resulting in less of a difference in reduction potential for the two subclusters. As noted above in the type **1** complexes, substitution of W for Mo results in a species that is more difficult to reduce by −130 mV while the substitution of Se for S has little effect (+10 mV). Displacement of the terminal ethanethiolate ligands with the less electron-donating groups such as arylthiolates and chloride ions results in double-cubanes which are significantly easier to reduce: *p*-chlorothiophenol, +160 mV; benzenethiol, +150 mV; Cl^-, +220 mV. This large influence of terminal ligand substitution has been noted in the sulfur double-cubanes and is understandable in light of the recently calculated electronic structure of $[MoFe_3S_4]^{3+}$ which predicts that reduction of the clusters occurs primarily on the Fe atoms [24]. Electron donation by terminal ligands onto the subcluster iron atoms makes it more difficult to reduce these iron atoms.

The great similarity of the redox behavior of the Se and S cubane clusters indicates that there would

be no obvious advantage to a biological system to substitute Se for S from the perspective of simple electron transfer processes. Therefore it is not surprising that to date Se in biological systems is found in selenocysteine [14]. There its different redox ability compared to sulfur (involving O atom transfer) is exploited in, for example, glutathione peroxidase [25].

Conclusions

In the present study we have demonstrated that both $MoSe_4^{2-}$ and WSe_4^{2-} undergo 'self-assembly' type reactions to produce double-cubane clusters. Three types of selenide-containing double-cubane complexes have been isolated, with two being structurally characterized by single-crystal X-ray diffraction experiments. All of the products show the full stoichiometric amount of four seleniums per cubane unit, indicating that MSe_4^{2-} can effectively deliver all four selenium atoms in the assembly process even though one is no longer covalently bound to M. The two structures are similar to the analogous sulfur double-cubanes, with the major structural difference being the more acute bridging Mo–Se–Fe angles within the subclusters. This allows for the incorporation of the larger selenide ions within cubane subclusters with the intracluster Fe····Mo and Fe···Fe distances changing only slightly. Several terminal thiolate displacement reactions on $[Mo_2Fe_7Se_8(SEt)_{12}]^{3-}$ have also been demonstrated.

Characterization techniques show several differences between the sulfur and selenium double-cubanes, although overall, the degree of similarity is unusual. Isotropic ^1H NMR shifts of terminal ligand protons in the complexes are analogous, with the selenides exhibiting larger isotropic shifts. This is in accord with the selenium analogs' larger room temperature solution magnetic susceptibilities. The larger magnetic moment demonstrates that the antiferromagnetic coupling in these complexes is more greatly effected by the larger metal-to-metal separations than by the greater covalency of the selenide superexchange bridges. Electrochemical properties of the selenium and sulfide double-cubanes are identical within experimental error, which is surprising in light of the greater electronegativity of sulfide relative to selenide. The electronic absorption spectra of the selenium double-cubanes are red-shifted slightly with respect to their sulfur analogs which is in accord with the expected influence of the less electronegative selenide upon these predominantly LMCT bands. No ^{77}Se NMR were obtained, presumably due to paramagnetic broadening.

Future work will be directed towards the synthesis of selenium mono-cubane complexes and the study of their reactivities towards nitrogenase substrates.

Supplementary material

A listing of thermal and atomic positional parameters (38 pages) and tables of structure factors (32 pages) are available from the authors on request.

References

1 (a) R. H. Holm, *Chem. Soc. Rev., 10* (1981) 455; (b) D. Coucouvanis, *Acc. Chem. Res., 14* (1981) 201.
2 T. E. Wolff, J. M. Berg, C. Warrick, K. O. Hodgson, R. H. Holm and R. B. Frankel, *J. Am. Chem. Soc., 100* (1978) 4630.
3 G. Christou, C. D. Garner and F. E. Mabbs, *Inorg. Chim. Acta, 28* (1978) L189.
4 W. H. Armstrong and R. H. Holm, *J. Am. Chem. Soc., 103* (1981) 6246.
5 W. H. Armstrong, P. K. Mascharak and R. H. Holm, *Inorg. Chem., 21* (1982) 1699.
6 J. A. Kovacs and R. H. Holm, *Inorg. Chem., 26* (1987) 702.
7 S. Ciurli, M. J. Carney, R. H. Holm and G. C. Papaefthymiou, *Inorg. Chem., 28* (1989) 2696.
8 A. Müller, U. Schimanski and J. Schimanski, *Inorg. Chim. Acta, 76* (1983) L245.
9 (a) S. C. O'Neal and J. W. Kolis, *J. Am. Chem. Soc., 110* (1988) 1971; (b) *Inorg. Chem., 28* (1989) 2780; (c) R. W. M. Wardle, C. H. Mahler, C.-N. Chau and J. A. Ibers, *Inorg. Chem., 27* (1988) 2790.
10 K. E. Howard, T. B. Rauchfuss and S. R. Wilson, *Inorg. Chem., 27* (1988) 1710.
11 A. Müller, U. Wienboker and M. Penk, *Chimia, 43* (1989) 50.
12 (a) R. W. M. Wardle, C.-N. Chau and J. A. Ibers, *J. Am. Chem. Soc., 109* (1987) 1859; (b) R. W. M. Wardle, S. Bhaduri, C.-N. Chau and J. A. Ibers, *Inorg. Chem., 27* (1988) 1747; (c) M. A. Ansari, C.-N. Chau, C. H. Mahler and J. A. Ibers, *Inorg. Chem., 28* (1989) 650; (d) M. A. Ansari, C. H. Mahler and J. A. Ibers, *Inorg. Chem., 28* (1989) 2669.
13 M. A. Bobrik, E. J. Laskowski, R. W. Johnson, W. O. Gillum, J. M. Berg, K. O. Hodgson and R. H. Holm, *Inorg. Chem., 17* (1978) 1402.
14 E. C. Wilhelmsen *et al.*, in J. E. Spillholz, J. L. Martin and H. E. Gathner (eds.), *Selenium in Biology and Medicine,* Avi, Westport, CT, 1981, Ch. 63.
15 D. F. Evans, *J. Chem. Soc.,* (1959) 2003.
16 D. H. Live and S. I. Chan, *Anal. Chem., 42* (1970) 791.
17 T. E. Wolff, J. M. Berg, P. P. Power, K. O. Hodgson and R. H. Holm, *Inorg. Chem., 19* (1980) 430.
18 R. D. Shannon and C. T. Prewitt, *Acta Crystallogr., Sect. B, 25* (1969) 925.
19 K. Endrich, E. Guffolz, O. Serhadle and M. L. J. Ziegler, *Organomet. Chem., 349* (1988) 323.

20 T. E. Wolff, J. M. Berg, K. O. Hodgson, R. B. Frankel and R. H. Holm, *J. Am. Chem. Soc., 101* (1979) 4140.

21 (a) G. Christou and C. D. Garner, *J. Chem. Soc., Dalton Trans.,* (1980) 2354; (b) T. E. Wolff, P. P. Power, R. B. Frankel and R. H. Holm, *J. Am. Chem. Soc., 102* (1980) 4694; (c) R. E. Palermo, P. P. Power and R. H. Holm, *Inorg. Chem., 21* (1982) 173.

22 R. H. Holm, W. D. Philips, B. A. Averill, J. J. Mayerle and T. Herskovitz, *J. Am. Chem. Soc., 96* (1974) 2109.

23 J. P. Jesson, in G. N. La Mar, W. D. Horrocks and R. H. Holm (eds.), *NMR of Paramagnetic Molecules: Principles and Applications,* Academic Press, New York, 1973, Ch. 1.

24 M. Cook and M. Karplus, *J. Chem. Phys., 83* (1985) 6344.

25 J. T. Rotruck, A. L. Pope, H. E. Ganther, A. B. Swanson, D. G. Hafeman and W. G. Hoekstra, *Science, 179* (1973) 588.